Targeted Car–Parrinello molecular dynamics: Elucidating double proton transfer in formic acid dimer

Phineus R. L. Markwick[a)]
European Molecular Biology Laboratory, Meyerhofstrasse 1, Heidelberg 69117, Germany

Nikos L. Doltsinis and Dominik Marx
Lehrstuhl für Theoretische Chemie, Ruhr-Universität Bochum, Bochum 44780, Germany

(Received 25 August 2004; accepted 5 November 2004; published online 20 January 2005)

The targeted molecular dynamics method, making possible the study of rare events, has been assessed in the framework of Car–Parrinello *ab initio* molecular dynamics. As a test case, we have studied the staggered–eclipsed rotation of ethane. The technique has subsequently been applied to investigate the nature of double proton transfer in formic acid dimer. The latter is found to follow a concerted transfer mechanism involving an essentially planar transition state. A ''funnel-like region'' of the potential energy surface is identified, where floppy intermolecular modes stiffen upon approaching the transition state. © *2005 American Institute of Physics.*
[DOI: 10.1063/1.1842049]

I. INTRODUCTION

Despite continuous advances in both numerical efficiency and computer technology, microcanonical Car–Parrinello molecular dynamics (CP-MD) simulations[1,2] are still limited to processes involving a few hundreds of atoms and occurring within a few tens of picoseconds at most. The number of chemical reactions which take place spontaneously on such a short time scale, however, is fairly limited; typically energy barriers of many kcal/mol need to be overcome. A wide variety of computational approaches has been developed over the years to force chemical reactions in *ab initio* molecular dynamics (MD). The fundamental problem in moving from reactants to products is that the true reaction coordinate is often unknown. Choosing a realistic reaction coordinate is essential for a simulation of rare events to be useful. This task becomes exceedingly difficult for systems with a large number of nuclear degrees of freedom. A way of systematically determining an ensemble of reaction coordinates has been suggested by Chandler and co-workers[3,4] based on pioneering work by Pratt.[5] Although powerful and appealing, their transition path sampling method is computationally rather demanding, in particular, when used in combination with CP-MD.[6] In the latter context, a variety of alternative methods have been proposed over the years, for instance, distance[7,8] and coordination[9–11] constraints, chemical flooding,[12] canonical adiabatic free energy sampling,[13] and non-Markovian metadynamics.[14,15]

In a limited number of cases, the reaction coordinate can be approximated reasonably well by simple geometric variables, such as bond lengths or angles. Rare events of this type may be studied using standard constraint techniques,[16–18] provided that one is able to guess the reaction mechanism prior to the simulation. The targeted molecular dynamics (TMD) approach proposed by Schlitter and co-workers[19–21] retains the simplicity of a distance constraint without the need to know in advance a good low-dimensional approximation to the reaction coordinate.

In the TMD method, the reaction coordinate is defined by a single mass-weighted root-mean-square ''target distance'' between a known initial structure and a fixed final (target) structure. By gradually reducing the constrained target distance to zero, the system is driven from the reactant to product state without explicitly defining the reaction pathway. During the course of a TMD simulation, in which the constraint target distance is reduced to zero, the system samples a reaction surface, rather than simply following the minimum energy path (MEP). TMD using classical force fields has recently been employed with considerable success to study conformational transitions and folding in proteins.[22–27]

In this paper we present the first example of TMD within the framework of CP-MD (Refs. 1, 2) for the study of chemical reactions involving transitions over a low energy barrier. We first apply the method to study the staggered-to-eclipsed-to-staggered conformational transition of ethane and demonstrate that *ab initio* TMD reproduces an accurate representation of the structural and energetic properties of this system along the reaction path. This system is particularly interesting as a test case since the reaction path is characterized by a high intrinsic symmetry in view of the nature of the staggered/eclipsed rotational transition.

We then employ targeted CP-MD simulations to study the nature of the double proton transfer (DPT) reaction in formic acid dimer (FAD). As a model system for hydrogen bonded nucleic acid base pairs, FAD continues to attract much attention from both experimental[28,29] and theoretical researchers;[30–36] see also references cited therein for review of earlier work. In particular, interpretation of recent high resolution spectroscopic measurements ''suggest that the proton transfer tunneling involves an out of plane motion of

[a)]Author to whom correspondence should be addressed. Fax: ++49 6221 387 306. Electronic mail: markwick@embl.de

the proton''[28] whereas simulations[32] questioned the concerted nature[37] of the DPT event in FAD. In this light, the issue of DPT in FAD warrants to be revisited using methods that neither impose a planar transition state nor a concerted mechanism *a priori*. Thus, only simulation techniques that allow for fluctuations, i.e., deviations from the MEP as driven by the finite temperature dynamics of the nuclear skeleton, are appropriate to address these aspects.

As the use of any constraint introduces a bias into the MD simulation, we have also studied the FAD system using a coordination constraint[9–11] and a simple distance constraint.[7,8] By comparing the results of these CP-MD simulations using different constraints, we attempt to identify structural phenomena associated with the DPT mechanism in FAD. In particular, the coordination and bond distance constraints have been applied asymmetrically, i.e., to only one hydrogen bond, in order to rule out any possible inherent bias towards concerted DPT.

II. METHODS

A. Targeted molecular dynamics

A detailed description of TMD including a discussion of the mechanical and statistical mechanical properties of the constraint is available in the literature.[20] Here, we simply provide a brief outline including the equations relevant to this work. In TMD, the reaction coordinate is defined as the target distance

$$D(\mathbf{R})=\left(\sum_{i=1}^{N}\mu_i^2(\mathbf{r}_i-\mathbf{t}_i)^2\right)^{1/2} \tag{1}$$

between the instantaneous reactant structure $\mathbf{R}=\{\mathbf{r}_i\}$ and the fixed product (target) structure $\mathbf{T}=\{\mathbf{t}_i\}$, $\mathbf{r}_i$ and $\mathbf{t}_i$ being the respective atomic positions. The mass weighting factor $\mu_i=m_i/M$ is the ratio of the mass of atom i, m_i, and the total mass of the system, M. In order to eliminate any translational or rotational contributions, the target distance $D(\mathbf{R})$ is minimized by superimposing the centers of mass of the two configurations $\mathbf{R}$ and $\mathbf{T}$ followed by rotation of the target structure. The remaining distance, called the target distance, is a measure of the structural root-mean-square distance between the two molecular conformations. During the course of the molecular dynamics simulation, this distance is gradually reduced towards zero and the initial reactant structure $\mathbf{R}$ is driven towards the target structure. A particularly attractive feature of this approach is the fact that the time averaged constraint force $\langle f\rangle_{D=\text{const}}$ obtained from a TMD run at a fixed value of D as the average Lagrange multiplier can be used directly to calculate the free energy difference

$$\Delta A=A(D_f)-A(D_i)=-\int_{D_i}^{D_f}\langle f\rangle_{D'}dD' \tag{2}$$

by thermodynamic integration from the initial to the final state, without the need to correct for metric tensor effects.[20] Figure 1 provides a pictorial representation of the initial and target structures for ethane and formic acid dimer that are used in this study.

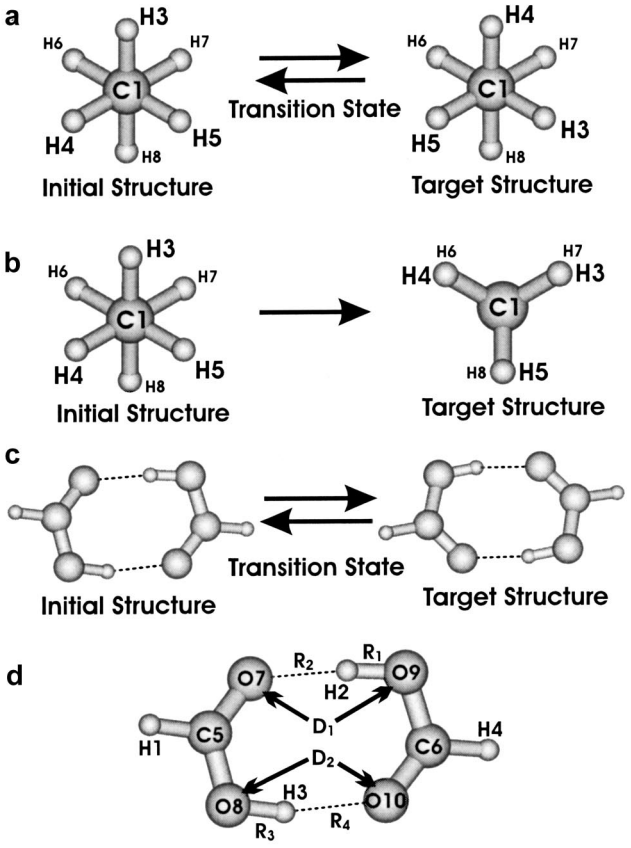

FIG. 1. (a) Initial and target ethane structures using the staggered conformation (rotation by 120°) as the target structure (see text for more details). (b) Initial and target ethane structures using the eclipsed conformation (rotation by 60°) as the target structure (see text for more details). (c) Initial and target FAD structures. (d) Initial structure of FAD with atoms and distances labeled.

B. Coordination constrained molecular dynamics

Interatomic distances may also be controlled in a more indirect and collective fashion by constraining the coordination number of a reactive center. There are several examples of coordination constrained MD available in the literature[9–11] to which we refer the reader for a detailed discussion of the underlying theory. The coordination center of interest in the present work is the oxygen atom O_8 (see Fig. 1). The hydrogen-specific coordination number n for this atom is given by

$$n=\sum_{i=1}^{N_\text{H}}[\exp(\kappa(r_i-r_c))+1]^{-1}, \tag{3}$$

where the summation is performed over all N_H (in this case 4) hydrogen atoms in the system, r_i is the distance between the oxygen atom O_8 and hydrogen atom i, r_c is the cutoff radius, and κ^{-1} determines the width of the distribution. Based on the MD averaged equilibrium structure of FAD, we chose a cutoff radius of $r_c=2.46$ a.u. and set $\kappa^{-1}=5.292$ a.u., which resulted in an equilibrium value of $n_e=0.956$ being sufficiently close to unity. The DPT reaction was driven by incrementally reducing the coordination num-

ber towards zero. Similar to the case of TMD described above, the free energy profile for the reaction is obtained by numerical integration,

$$\Delta A = A(n_f) - A(n_i) = -\int_{n_i}^{n_f} \langle f \rangle_{n'} dn'. \quad (4)$$

However, in contrast to TMD, in this case the time-averaged mean force $\langle f \rangle_{n=\text{const}}$ is not identical to the average constraint force, the latter having to be corrected for metric effects.[9] All results presented in this paper include these corrections.

C. Bond distance constrained molecular dynamics

The last constraint employed in this work to study the DPT process in FAD is a simple distance constraint.[16] The constraint was applied to the interatomic distance between atoms O_8 and H_3. Starting with a constraint O–H bond distance of 1.885 a.u. for the equilibrium structure of FAD, the O–H bond distance was gradually increased in order to drive the reaction. Like the more general target distance constraint, this simple bond length constraint also has the advantage that the mean force is a straightforward average of the constraint force, i.e., the Lagrange multiplier.[18]

D. Computational details

In the course of this study, we have concentrated on two activated processes: the staggered–eclipsed–staggered conformational transition in ethane and the DPT reaction in FAD as shown in Fig. 1. In both systems we have employed TMD based on CP-MD (Refs. 1, 2) (T-CP-MD). Additionally, for the study of FAD, we have also performed coordination constrained and simple distance constrained CP-MD. The general procedure for all constrained CP-MD simulations is identical. Starting with a geometrically optimized structure for the system of interest, the system was placed at the center of a periodically repeating cubic box of length $L=15$ a.u. for ethane and $L=25$ a.u. for FAD. The system was first slowly brought to thermodynamic equilibrium at 300 K using a Nosé-Hoover thermostat on the ions. A fictitious mass of 400 a.u. was ascribed to the electronic degrees of freedom and the coupled equations of motion for atomic nuclei and molecular orbitals were solved using the velocity Verlet algorithm with a time step of 4 a.u. For each nuclear configuration, the Kohn-Sham equations were solved using the Becke (B) exchange[38] and Lee, Yang, and Parr (LYP) correlation[39] functional. Core electrons were treated using the norm-conserving pseudopotentials of Troullier and Martins.[40] The valence orbitals were expanded in a plane-wave basis up to an energy cutoff of 70 Ry. Unconstrained CP-MD simulations were performed over 2 ps. After this equilibration period, the relevant constraint was switched on. For the T-CP-MD simulations, the nuclear coordinates of the system at each step in the simulation were first superimposed on the target structure in order to minimize the target distance D using a mass-weighted least-squares-fit algorithm.[41] The target structures for both the ethane and FAD systems (see Fig. 1) were obtained from an unconstrained CP-MD simulation, i.e., they differ from the optimized 0 K geometries. A series of T-CP-MD runs were performed at fixed values of D. For each D, the system was first brought to thermodynamic equilibrium at 300 K, and the electronic wave functions were repeatedly quenched onto the Born-Oppenheimer surface. After stabilizing the system at a given D, the Nosé-Hoover thermostat on the nuclei was switched off and a 0.5 ps constrained CP-MD simulation was performed. All calculations were performed using the CPMD package.[2,42]

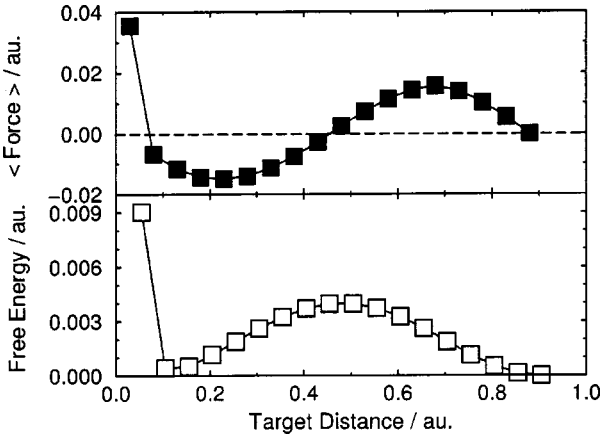

FIG. 2. Variation of the average constraint force (top) and free energy profile (bottom) as a function of D for the staggered–eclipsed–staggered transition in ethane using T-CP-MD; see Fig. 1(a).

III. RESULTS AND DISCUSSION

A. Ethane: Staggered–eclipsed–staggered internal rotation

The average constraint force for the staggered-to-eclipsed-to-staggered conformational transition (rotation by 120°) in ethane is shown in Fig. 2 as a function of the target distance including the associated free energy profile. A pictorial representation of the initial and target structures used in this simulation is shown in Fig. 1(a). The initial target distance between the two staggered conformations is $D=0.88$ a.u. corresponding to a rotational angle about the C–C axis of 120°. At this initial D, the average constraint force is approximately zero. As D decreases, the constraint force increases as the constraint pushes the system towards the energetically unfavorable eclipsed conformation (rotation by 60°). Having reached a maximum, the average constraint force then returns to zero at the transition state ($D=0.43$ a.u.). At this point, the system is sitting exactly on the top of the potential energy barrier. Further reduction of D results in negative values of the average constraint force. This arises from the fact that, having overcome the energy barrier, the system would preferentially move directly to the staggered (target) structure. The constraint however does not allow this, and acts in such a way as to ''pull'' or ''hold'' the system away from the target structure, resulting in a negative average constraint force. As D gets very close to zero, the average force adopts exceedingly large positive values. This is because the phase space volume available to the system decreases with D resulting in an increasing centrifugal component of the constraint force.[20] In other words, when the available phase space becomes so small that it confines the

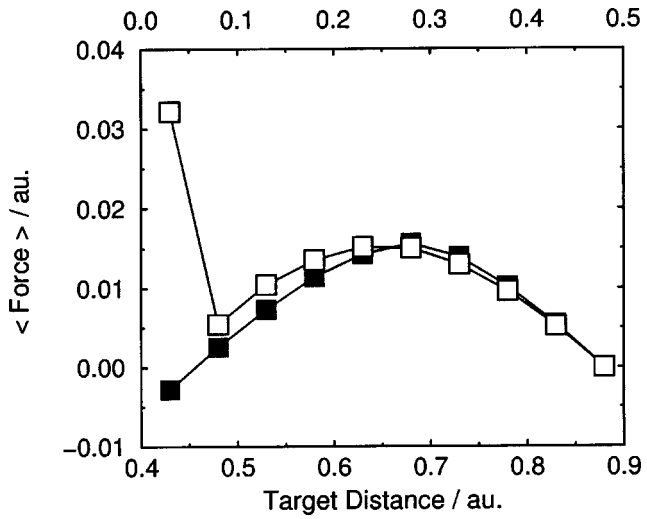

FIG. 3. Comparison of the average constraint force function using a staggered (120° rotation, filled squares) and eclipsed (60° rotation, open squares) target structure of ethane, see Figs. 1(a) and 1(b), respectively. The target distance on the lower *x* axis is for the staggered target structure and the upper *x* axis is for the eclipsed target structure. Even at relatively large target distances the effect of the target constraint entropy is clearly visible.

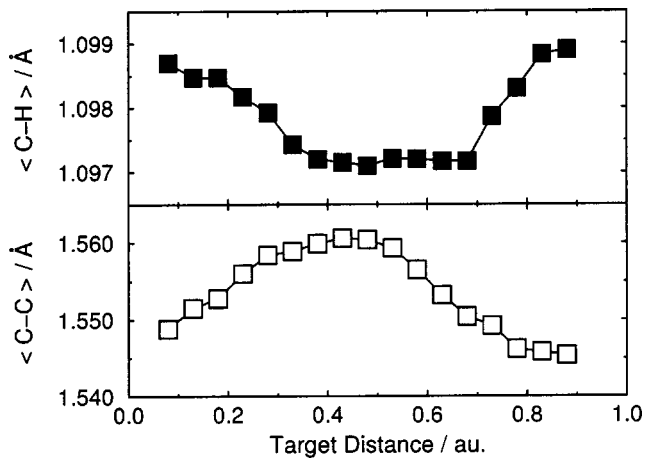

FIG. 4. Variation of the average C–H (top) and average C–C (bottom) bond length as a function of *D* for the staggered target structure (120° rotation) of ethane. In the vicinity of the eclipsed region, a decrease in the average C–H bond length and an increase in the C–C bond length is clearly visible. This is due to the effect of steric interaction of the two methyl groups.

vibrations of the system, the average constraint force increases dramatically as a result of this ''entropy loss.'' The free energy profile resembles a Gaussian form, with a maximum at approximately the midpoint of the reaction coordinate. Indeed the resulting free energy profile is very similar to that obtained from the MEP. At $D \approx 0.03$ a.u., the free energy dramatically increases. This is the ''target constraint entropy'' that dominates the free energy profile when *D* becomes so small that it interferes with the vibrations of the system.[20]

The effect of the target constraint entropy when *D* becomes very small is readily observable. However, in principle, over the entire reaction coordinate the available conformational space is continuously being reduced as the target distance is monotonically decreased. One interesting question that arises is then: Does the reduction in the available conformational space on decreasing *D* affects the free energy profile of the reaction at larger *D* or only when it becomes extremely small? In order to answer this question, we have performed a second T-CP-MD simulation, this time using a target structure that lies very close to the eclipsed state [see Fig. 1(b)] corresponding to a rotation of 60°. For the target structure we used one of the sampled structures from the initial TMD simulation at $D = 0.43$ a.u. Using the same initial structure as in the first TMD run, we calculated the average constraint force as a function of the new *D*. Figure 3 shows the comparison between the two average constraint force curves, which have been superimposed. We observe that the effect of the targeted constraint entropy is apparent at *D* as large as 0.2 a.u. This important result suggests that one must be careful when comparing the free energy profile obtained by TMD with experimental activation energies. While the enthalpic contribution to the free energy profile is predominantly dependent on the choice of electronic structure approach, the entropic contribution to the free energy profile is affected by the choice reaction coordinate, i.e., the target structure. However, we would like to point out that for any particular reaction coordinate (prescribed by TMD with a particular target structure) the free energy differences obtained by thermodynamic integration are free from artifacts despite the steep increase in constraint force near $D = 0$. Merely the connection to experiment can be complicated by the fact that the phase space volume in TMD is not constant. Nevertheless, our present example (Fig. 3) illustrates that integration of the mean force sufficiently far away from $D = 0$ is essentially independent of the choice of target structure.

One of the main reasons for performing this initial study on ethane was to establish whether T-CP-MD accurately reproduces changes in the structural properties of the system during the conformational transition. It is well-known that due to increased ''steric interaction'' between the two methyl groups, the C–C bond length in ethane is slightly larger in the eclipsed than in the staggered conformation. For identical reasons, the C–H bond in the eclipsed conformation is slightly shorter than in the staggered conformer. Figure 4 shows the change in the mean C–C and mean C–H bond lengths as a function of *D*. As can be seen, the expected changes in the structure described above are observed in the T-CP-MD simulation. We observe that the mean C–C bond length increases by 0.015 Å from 1.545 Å to 1.560 Å, while the mean C–H bond length decreases by 0.002 Å from 1.099 Å to 1.097 Å. These subtle changes are very similar to those found when comparing the optimized ground state and transition state structures. On the MEP we observe an increase in the C–C bond length of 0.013 Å from 1.541 Å to 1.554 Å and a decrease in the C–H bond length of 0.001 Å from 1.096 Å to 1.095 Å.

B. Formic acid dimer: Energetics

We performed two series of T-CP-MD simulations for the study of DPT in FAD. In the first series of simulations we used a full target constraint including all atoms of the molecule, while in the second simulation we employed a ''par-

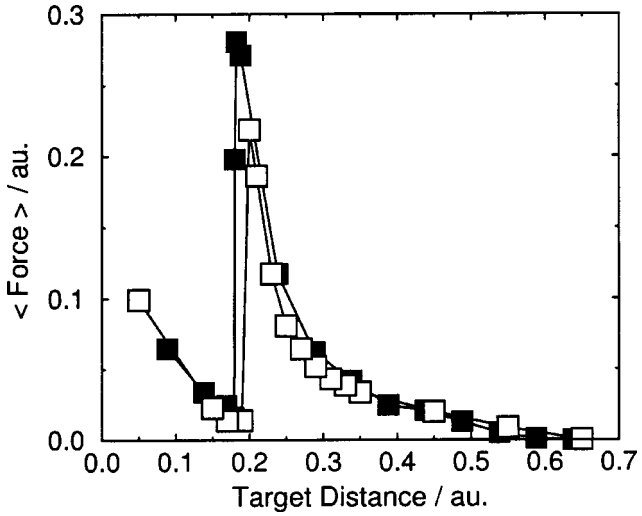

FIG. 5. Variation in the average constraint force as a function of D for FAD. Filled squares represent the average constraint force for the full TMD, while the open squares show the result for the partial target structure involving only the four oxygen atoms and the two protons involved in DPT. After the DPT event ($D=0.2$ a.u.) the constraint loses control of the system.

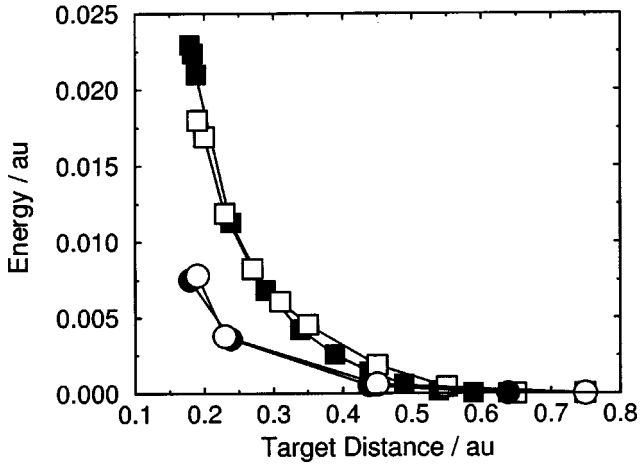

FIG. 6. Free energy and enthalpy profiles approaching the transition state. The free energy barrier to DPT for full TMD (filled squares) is larger than that for partial TMD (open squares). This arises only from a difference in the entropic contribution to the free energy. The enthalpy profiles for the full TMD (filled circles) and partial TMD (open circles) are almost identical.

tial'' target constraint, only using for the evaluation of D those atoms that are predominantly involved in the DPT reaction, i.e., the four oxygen atoms and two protons constituting the two H bonds. The resulting average constraint force curves are depicted in Fig. 5. In both cases, we see a very different force curve compared to that obtained in the ethane simulation. The average constraint force increases slowly to a maximum as the DPT event is reached. Just after DPT, the average constraint force decreases rapidly to zero. At very small D, the average constraint force begins to increase again, due to the effect of the target constraint entropy. It is immediately apparent that in FAD, the constraint ''loses control'' of the system after the DPT reaction has occurred. We consider that this is partially due to the fact that FAD is much more flexible than ethane and partially due to the fact that the mass-weighted TMD constraint is not ''focused'' directly on the protons involved in DPT. In light of this, we concentrate in the following on the reaction coordinate region up to the DPT event. The associated free energy and enthalpy profiles are shown in Fig. 6. As can be seen, the free energy barrier to proton transfer is slightly but systematically larger for the full TMD than in the partial TMD simulation. This is due to a difference in the entropy of the system. In order to assess this more quantitatively we have calculated for both target constraints at certain target distances the entropy of the system in the quasiharmonic limit following Refs. 43, 44. Quasiharmonic frequencies ω_i were calculated from the mass-weighted covariance matrix and inserted in the entropy formula[44]

$$S_{\mathrm{ho}}=k\sum_{i}^{3N-6}\frac{\hbar\omega_i/kT}{e^{\hbar\omega_i/kT}-1}-\ln(1-e^{-\hbar\omega_i/kT}). \tag{5}$$

In this way, we calculated the change in entropy of the system as a function of D within the quasiharmonic approximation. The entropy profile includes both the entropy change of the physical system and the target constraint entropy. We found that on performing T-CP-MD simulations at a given D over different time scales (0.5 ps, 1.0 ps, 1.5 ps, and 2.0 ps), there was very little change in the average constraint force, but significant differences in the quasiharmonic entropy values. We performed for a few target distances longer simulations over 2.0 ps in order to get a more accurate approximation of the associated entropy value. From the free energy and entropy profiles, we have obtained an estimate for the enthalpy profile for the two T-CP-MD runs. We note that the enthalpy profile is only approximate as Eq. (5) has been derived for the canonical ensemble. The enthalpy profile in the partial and full T-CP-MD runs are ostensibly identical (see open and filled circles in Fig. 6), and very similar to the ''static'' transition state enthalpy value of 0.086 a.u. (22.6 kJ/mol) obtained from the Kohn-Sham energy difference between the optimized equilibrium and transition state structures. The difference between the partial and full T-CP-MD free energy profiles arises only due to the difference in the entropy contribution from the two different target constraints. Indeed, this is the only significant difference that we observed between the partial and full TMD runs.

The average constraint force curves and associated free energy and enthalpy profiles for the coordination constraint and distance constraint simulations are shown in Figs. 7 and 8. Similar to the case of TMD, these constraints also lose control of the system after the DPT event. Despite the fact that the functional form of the average constraint force curves and free energy curves are different for the different constraints, the enthalpy of the reaction in each case appears to be very similar. The specific value of the energy barrier to DPT obtained in these constrained CP-MD simulations is determined by the electronic structure method chosen and not by the type of constraint employed. Indeed there are many studies concerning the exact value of the energy barrier to DPT available in the literature. The BLYP functional gives a very low energy barrier (22.6 kJ/mol) compared to more accurate post-Hartree-Fock CISD (Q) calculations (45.2 kJ/mol).[31] Unfortunately such post-Hartree-Fock meth-

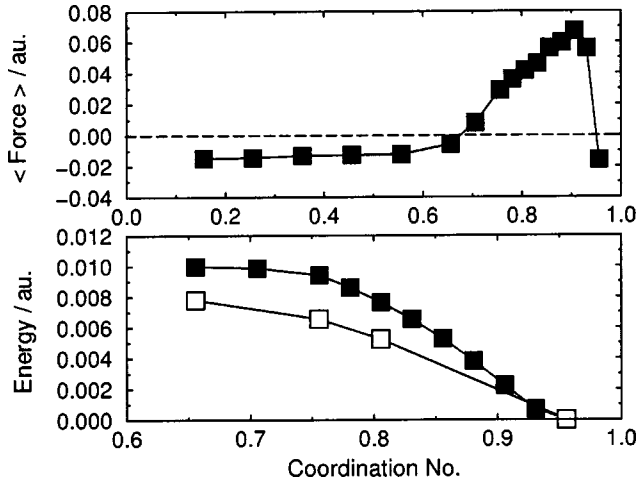

FIG. 7. Upper panel, average constraint force as a function of coordination number for coordination constrained CP-MD of FAD. Lower panel, associated free energy (filled squares) and enthalpy (open squares) profiles.

ods cannot be readily used in a constrained CP-MD simulation due to the excessive CPU time required. However, according to a most recent study[36] the barrier height is only 33.1 kJ/mol (7.9 kcal/mol), much closer to the BLYP value than previously thought.

Highly accurate theoretical estimates of the barrier to DPT, i.e., the energy of the transition state relative to the equilibrium structure, are more readily obtained from static calculations of the MEP. Constrained CP-MD simulations, however, provide an insight into changes in the structural properties of the system across the reaction coordinate at finite temperature, i.e., including fluctuations. This is the topic of the following section.

C. Formic acid dimer: Structural changes and mechanism

In this section, we discuss the changes in the structural properties of the FAD system as it approaches the DPT event. All three constraints liberated a concerted DPT

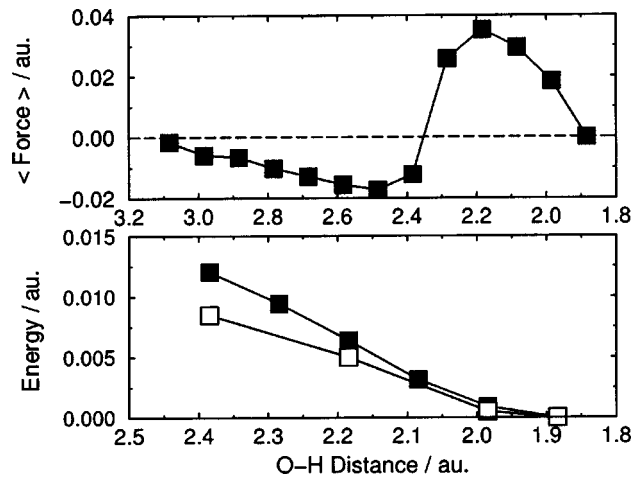

FIG. 8. Upper panel, average constraint force as a function the O–H distance for distance constrained CP-MD of FAD. Lower panel, associated free energy (filled squares) and enthalpy (open squares) profiles.

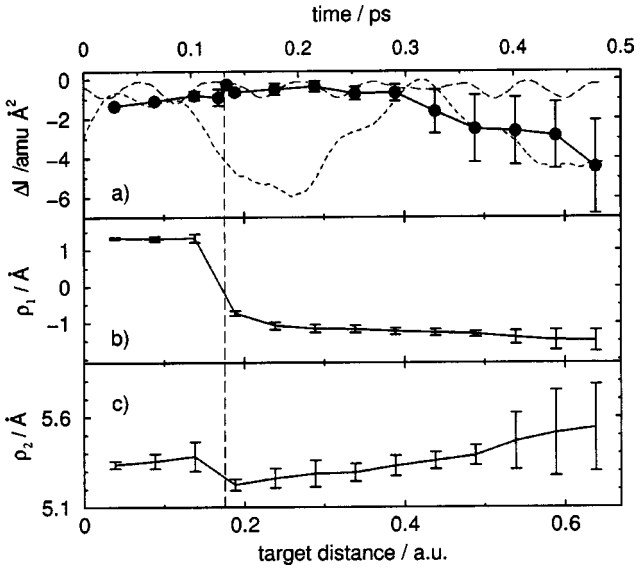

FIG. 9. FAD T-CP-MD: $\langle \Delta I \rangle$ (a), $\langle \rho_1 \rangle$ (b), and $\langle \rho_2 \rangle$ (c) as a function of D (——). The error bars indicate the respective σ. At large D, the system exhibits large amplitude oscillations about a heavily nonplanar structure. On approaching the transition state (vertical dashed line), the amplitude of these oscillations decreases dramatically accompanied by an increase in frequency and planarity [see (a) for $\Delta I(t)$ at $D=0.59$ a.u. (- - - -) and $D=0.24$ a.u. (– – – –)].

mechanism. This is a very important result, as none of the constraints employed intrinsically enforce a concerted reaction mechanism. In the coordination and distance constraint simulations, multiple DPT events were observed at the transition state. For the TMD simulations, only a single concerted DPT event was observed, after which the system immediately relaxed towards the equilibrium ground state geometry. Quantum chemistry calculations suggest that the transition state is planar with D_{2h} symmetry.[31] We first investigated how close to planarity the system gets as it approaches the transition state. One of the most sensitive measures of the planarity of the system is the inertia defect ΔI which is defined as

$$\Delta I = I_C - I_B - I_A , \tag{6}$$

where $I_C > I_B > I_A$ are the principle moments of inertia of the system; note that this definition is consistent with the ΔI data reported in Ref. 28. The inertia defect is a convenient measure of the planarity of the system since $\Delta I \equiv 0$ for completely planar molecules. Figure 9(a) shows the change in the average $\langle \Delta I \rangle$ and root-mean-square fluctuations $\sigma(\Delta I)$ of ΔI as a function of the constraint for the T-CP-MD simulation. $\langle \Delta I \rangle$ tends towards zero at the transition state, but, on average, never actually gets to exactly zero. However, $\langle \Delta I \rangle$ does not decrease monotonically. We observe an initial rapid increase in $\langle \Delta I \rangle$ long before the transition state is reached. As the system approaches the transition state, $\langle \Delta I \rangle$ remains almost invariant, only increasing slightly. $\sigma(\Delta I)$ exhibits a similar quasiplateau. These results suggest that in the equilibrium structure, FAD undergoes slow large amplitude fluctuations causing the dimer to deviate strongly from its optimized planar geometry. On approaching the transition state, however, the system undergoes a stiffening of the out-of-

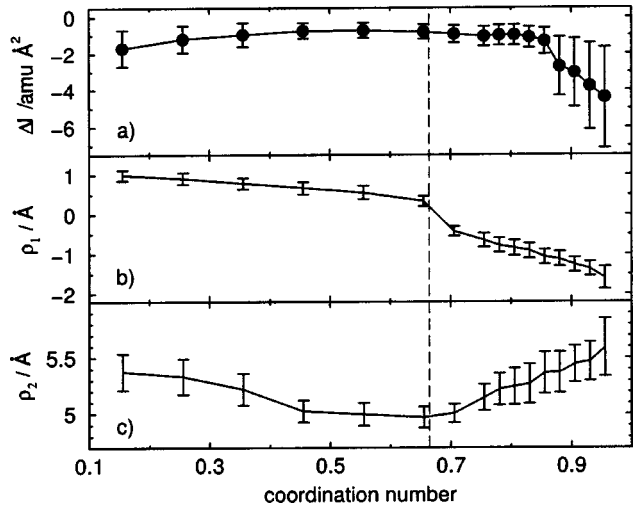

FIG. 10. FAD coordination constraint CP-MD: $\langle \Delta I \rangle$ (a), $\langle \rho_1 \rangle$ (b), and $\langle \rho_2 \rangle$ (c) as a function of the coordination number. The error bars indicate the respective σ. DPT occurs at the vertical dashed line.

plane vibrations. The system enters a funnel-like region of the potential energy surface which results in a dramatic decrease of the amplitude of the oscillation of ΔI and an increase in the frequency of oscillation upon approaching the transition state region where DPT occurs. This is shown explicitly in Fig. 9(a). A similar effect is seen for the coordination constraint shown in Fig. 10(a) and the distance constraint. However, after the DPT reaction has occurred, we see very different behavior in ΔI for the target and coordination constraints. In the case of T-CP-MD, $\langle \Delta I \rangle$ decreases and $\sigma(\Delta I)$ increases just after the reaction as expected. Only as D is reduced further, due to the fact that the constraint now drives the system towards a fixed target structure, $\langle \Delta I \rangle$ goes to -1.37 amu Å^2 which is the value of ΔI for the (nonplanar) target structure, see Sec. II D, and $\sigma(\Delta I)$ goes to zero. In the coordination constraint, however, the planarity of the system continues to increase slightly after the DPT reaction has occurred. This is an artifact of the coordination constraint, which is now acting predominantly on the newly formed H bond. The flexibility of the FAD system is due to the flexibility of the two H bonds. The coordination constraint acting on one of the H bonds induces planarity even after the reaction has occurred. As the coordination constraint is further reduced to zero, the newly formed H-bond length is allowed to increase slowly and the average planarity of the system in turn also slowly decreases. A similar argument can be applied to the variation in $\sigma(\Delta I)$ for this constraint.

Following the work of Miura *et al.*,[31] we have extended our analysis of the properties of FAD by studying two symmetry-adapted generalized coordinates[30]

$$\rho_1 = R_1 - R_2 + R_3 - R_4, \tag{7}$$

$$\rho_2 = D_1 + D_2, \tag{8}$$

see Fig. 1 for definitions of variables. The ρ_1 coordinate characterizes synchronized hydrogen motion, while ρ_2 describes the intermolecular vibrations; note that ρ_1 and ρ_2 are the standard coordinates used to describe a H bond, i.e., the asymmetric stretch and the donor-acceptor distance, generalized to two H bonds. Figure 9(b) shows the change in the average, $\langle \rho_1 \rangle$ and root-mean-square fluctuations $\sigma(\rho_1)$ of ρ_1 for the target and coordination constrained simulations. For the case of T-CP-MD, we see that ρ_1 decreases slowly in the initial stages of the reaction. Very close to the transition state, we observe a distinct discontinuity and $\langle \rho_1 \rangle$ becomes zero at the transition state and large and positive shortly after the reaction has occurred. One of the reasons for this large discontinuity is that after DPT, the target constraint loses control over the system, which moves almost directly into the equilibrium ground state structure. A similar effect is observed for the coordination constraint shown in Fig. 10(b). The discontinuity is much smaller here, which is at least in part due to the fact that the constraint controls the system somewhat better than the target constraint after the reaction has occurred. The change in $\sigma(\rho_1)$ is much more interesting. For both constraints, we observe a distinct decrease in $\sigma(\rho_1)$ long before the transition state is reached. After a plateau, $\sigma(\rho_1)$ decreases again very close to the transition state. Similar to our previous discussion for ΔI, it appears that the system enters a rather rigid funnel region of the potential energy surface in the very early stages of the DPT reaction, which is maintained until concerted DPT occurs. In both cases $\rho_1 = 0$ at the transition state signaling concerted DPT; similar results were obtained for the distance constraint. This result is particularly interesting, since, unlike in previous studies,[31] none of the constraints employed here implicitly favors a concerted mechanism.

The change in $\langle \rho_2 \rangle$ and $\sigma(\rho_2)$ for the target and coordination constrained simulations is shown in Figs. 9(c) and 10(c), respectively. For both constraints we see a smooth decrease in $\langle \rho_2 \rangle$ as the system approaches the transition state. The minimum of $\langle \rho_2 \rangle$ just prior to the DPT reaction is slightly larger in the case of T-CP-MD (5.22 Å) than for the coordination constraint (5.01 Å). In the distance constraint the minimum $\langle \rho_2 \rangle$ just prior to the transition state is even smaller (4.97 Å). The reason for the rather large value obtained in T-CP-MD simulations is due to the fact that the frozen target structure (corresponding to a fixed value of $\rho_2 = 5.32$ Å) influences the structural changes. Particularly as D gets small, the system is driven towards the specifically defined target structure. In all three constrained CP-MD simulations we see however that $\sigma(\rho_2)$ decreases rapidly initially before stabilizing and then decreases again on close approach to the transition state. In line with the previously presented results for ΔI and ρ_1 this suggests that in the early stages of the reaction the dimer contracts and enters a funnel-like region of the potential energy surface (being characterized by high-frequency small-amplitude oscillations of intermolecular modes in comparison to the situation close to the equilibrium structure) which is maintained until the DPT process occurs. For the T-CP-MD simulations, the ρ_2 coordinate increases rapidly just after DPT and the system becomes more flexible. As D is reduced further $\langle \rho_2 \rangle$ tends towards the target structure value of 5.32 Å and $\sigma(\rho_2)$ decreases to zero. In the coordination constraint, $\langle \rho_2 \rangle$ continues to decrease after the DPT before slowly increasing again. Just as in the case of

ΔI, this effect is an artifact of the coordination constraint which is now acting strongly on the newly formed H bond.

IV. CONCLUSIONS

In this paper we have presented the first example of targeted Car-Parrinello molecular dynamics to study chemical reactions over low potential energy barriers. We have concentrated on two activated processes occurring within small molecules: the staggered–eclipsed–staggered conformational transition in ethane and the double proton transfer reaction in formic acid dimer. In the very small and rigid ethane test system we have observed that T-CP-MD accurately reproduces many of the known properties of the system associated with the conformational transition. In the case of FAD, a much more flexible system, the target constraint is less well suited to control the motion of the transferring protons. Due to the use of a mass-weighted target distance, TMD predominantly acts on the heavy atom frame. With regard to future applications of T-CP-MD, we are therefore optimistic as far as, for instance, *ab initio* simulations of conformational changes in complex systems are concerned. However, the present work has certainly shown the limitations of TMD in the context of proton transfer reactions. Nevertheless, the overall performance of TMD in the case of FAD is comparable to other simple geometric constraints such as a bond distance or coordination constraint.

Concerning FAD in particular, the aim of this study has been to characterize the entropic dynamic effects, which might lead to *qualitative* deviations of the finite temperature reaction path compared to the zero temperature minimum energy path. In this respect, it is worth noting that, despite not implicitly favoring a symmetrical proton transfer path, all constraints employed here have reproduced the concerted DPT as predicted by the MEP approach which neglects finite temperature fluctuations of the nuclear skeleton. Furthermore, we have shown that dynamical fluctuations are responsible for the inertia defect being nonzero throughout the reaction, at variance with predictions based on the MEP, and in particular slightly negative close to the transition state. This observation might offer a way to reconcile high-accuracy spectroscopic data[28] with previous quantum chemical calculations based on the MEP.

ACKNOWLEDGMENTS

The authors are grateful to J. Schlitter for helpful comments on this TMD technique and to M. Havenith for stimulating discussions on FAD.

[1] R. Car and M. Parrinello, Phys. Rev. Lett. **55**, 2471 (1985).
[2] D. Marx and J. Hutter, in *Modern Methods and Algorithms of Quantum Chemistry*, edited by J. Grotendorst (NIC, Jülich, 2000), www.theochem.rub.de/go/cprev.html
[3] D. Chandler, in *Classical and Quantum Dynamics in Condensed Phase Simulations*, edited by B. J. Berne, G. Ciccotti, and D. F. Coker (World Scientific, Singapore, 1998).
[4] P. G. Bolhuis, D. Chandler, C. Dellago, and P. L. Geissler, Annu. Rev. Phys. Chem. **53**, 291 (2002).
[5] L. R. Pratt, J. Chem. Phys. **85**, 5045 (1986).
[6] P. L. Geissler, C. Dellago, D. Chandler, J. Hutter, and M. Parrinello, Science **291**, 2121 (2001).
[7] A. Curioni, M. Sprik, W. Andreoni, H. Schiffer, J. Hutter, and M. Parrinello, J. Am. Chem. Soc. **119**, 7218 (1997).
[8] E. J. Meijer and M. Sprik, J. Am. Chem. Soc. **120**, 6345 (1998).
[9] M. Sprik, Chem. Phys. **258**, 139 (2000).
[10] J. E. Davies, N. L. Doltsinis, A. J. Kirby, C. D. Roussev, and M. Sprik, J. Am. Chem. Soc. **124**, 6594 (2002).
[11] N. L. Doltsinis and M. Sprik, Phys. Chem. Chem. Phys. **5**, 2612 (2003).
[12] E. M. Müller, A. de Meijere, and H. Grubmüller, J. Chem. Phys. **116**, 897 (2002).
[13] J. VandeVondele and U. Röthlisberger, J. Phys. Chem. B **106**, 203 (2002).
[14] A. Laio and M. Parrinello, Proc. Natl. Acad. Sci. U.S.A. **99**, 12562 (2002).
[15] M. Iannuzzi, A. Laio, and M. Parrinello, Phys. Rev. Lett. **90**, 238302 (2003).
[16] J. P. Ryckaert, G. Ciccotti, and H. J. C. Berendsen, J. Comput. Phys. **23**, 237 (1977).
[17] E. A. Carter, G. Ciccotti, J. T. Hynes, and R. Kapral, Chem. Phys. Lett. **156**, 472 (1989).
[18] M. Sprik and G. Ciccotti, J. Chem. Phys. **109**, 7737 (1998).
[19] J. Schlitter, M. Engels, P. Krüger, E. Jacobi, and A. Wollmer, Mol. Simul. **10**, 291 (1993).
[20] J. Schlitter, W. Swegat, and T. Mülders, J. Mol. Model. [Electronic Publication] **7**, 171 (2001).
[21] J. Schlitter and M. Klähn, Mol. Phys. **101**, 3439 (2003).
[22] B. Wroblowski, J. Diaz, J. Schlitter, and Y. Engelborghs, Protein Eng. **10**, 1163 (1997).
[23] O. Roche and M. Field, Protein Eng. **12**, 285 (1999).
[24] P. Fererra, J. Apostolakis, and A. Calfisch, J. Phys. Chem. B **104**, 4511 (2000).
[25] P. Fererra, J. Apostolakis, and A. Calfisch, Proteins **39**, 252 (2000).
[26] P. Kruger, S. Verheyden, P. Declerck, and Y. Engelborghs, Protein Sci. **10**, 798 (2001).
[27] Y. Kong, Y. Shen, T. Warth, and J. Ma, Proc. Natl. Acad. Sci. U.S.A. **99**, 5999 (2002).
[28] F. Madeja and M. Havenith, J. Chem. Phys. **117**, 7162 (2002).
[29] V. V. Matylitsky, C. Riehn, M. F. Gelin, and B. Brutschy, J. Chem. Phys. **119**, 10553 (2003).
[30] N. Shida, P. F. Barbara, and J. Almlöf, J. Chem. Phys. **94**, 3633 (1991).
[31] S. Miura, M. E. Tuckerman, and M. L. Klein, J. Chem. Phys. **109**, 5290 (1998).
[32] H. Ushiyama and K. Takatsuka, J. Chem. Phys. **115**, 5903 (2001).
[33] M. Meuwly, A. Müller, and S. Leutwyler, Phys. Chem. Chem. Phys. **5**, 2663 (2003).
[34] J. Chocholoušová, V. Špirko, and P. Hobza, Phys. Chem. Chem. Phys. **6**, 37 (2004).
[35] C. S. Tauterinann, A. F. Voegele, and K. L. Liedl, J. Chem. Phys. **120**, 631 (2004).
[36] C. S. Tautermann, M. J. Loferer, A. F. Voegele, and K. L. Liedl, J. Chem. Phys. **120**, 11650 (2004).
[37] R. L. Schowen, Angew. Chem., Int. Ed. Engl. **36**, 1434 (1997).
[38] A. D. Becke, Phys. Rev. A **38**, 3098 (1988).
[39] C. Lee, W. Yang, and R. C. Parr, Phys. Rev. B **37**, 785 (1988).
[40] N. Troullier and J. Martins, Phys. Rev. B **43**, 1993 (1991).
[41] A. D. McLachlan, Mol. Phys. **8**, 39 (1964).
[42] J. Hutter, P. Ballone, M. Bernasconi *et al.*, CPMD 3.4, MPI für Festkörperforschung, and IBM Zurich Research Laboratory, Stuttgart, 2001.
[43] J. Schlitter, Chem. Phys. Lett. **215**, 617 (1993).
[44] I. Andricioaei and M. Karplus, J. Chem. Phys. **115**, 6289 (2001).